JOURNAL OF SPACECRAFT AND ROCKETS
Vol. 35, No. 2, March–April 1998

Control of Thermal Deformations of Spherical Mirror Segment

Rakesh K. Kapania,* P. Mohan,† and A. Jakubowski‡
Virginia Polytechnic Institute and State University, Blacksburg, Virginia 24061-0203

Control of thermal deformations of a thin hexagonal spherical mirror segment using discrete and distributed actuators is presented. To determine the effectiveness of the actuators in controlling the thermal deformations of the mirror segment, a comparative study is conducted using two different models of the mirror–actuator system: 1) the mirror mounted on kinematic supports and controlled by piezoelectric strips bonded to the rear surface of the mirror and 2) the mirror mounted on force actuators, which are used to support the mirror as well as to control the surface deformations of the mirror. The performance of evenly distributed strips and that of strips placed at near-optimal locations obtained using heuristic integer programming are also compared. Both the force actuators and the piezoelectric strips are found to be equally effective in controlling the surface deformations of the mirror. A major drawback of the force actuators is the increase in the overall weight of the system, which is undesirable for space applications. On the other hand, the piezoelectric strips are very lightweight, and hence a large number of such strips can be used to control the surface distortions of the mirror, without imposing a weight penalty. The piezoelectric strips appear to be promising candidates for static shape control of flexible structures in space.

Nomenclature

b = side of graphite/epoxy plate, m
d_{33} = piezoelectric strain constant, m/V
E = root mean square error of the mirror surface distortions
f_j = control inputs (force applied to the force actuators or the voltage applied to the piezoelectric strips)
h = thickness of graphite/epoxy plate, m
m = number of nodes of the finite element model
n = number of force actuators or piezoelectric strips
u = correction to the transverse displacement
W = middeflection of graphite/epoxy plate, m
α_{ij} = influence coefficients
ψ = deformed shape (transverse displacement) of the mirror

Introduction

ONE of the most stringent requirements in the design of astronomical telescopes is the maintenance of the primary mirror surface to a very high degree of accuracy. The shape of the primary mirror has to be continuously monitored, and any deviation from the desired shape caused by external disturbances needs to be controlled by applying corrective measures. Active control techniques are being widely adopted to correct the surface inaccuracies of optical surfaces. This involves correction of the surface deformation by applying control inputs using discrete or distributed actuation. In the case of discrete actuation, concentrated forces are applied at discrete locations on the deformed mirror using actuators that are located at the rear surface of the mirror. In the case of distributed actuation, strips of piezoelectric material are used as actuators. These strips are either bonded to the rear surface of the mirror or embedded in a composite mirror faceplate. Piezoelectric materials undergo mechanical deformation when an electric field is applied. The resulting induced distributed strain is used to control the surface deformation of the structure.

Presented as Paper 96-4154 at the AIAA/USAF/NASA/ISSMO 6th Symposium on Multidisciplinary Analysis and Optimization, Bellevue, WA, Sept. 4–6, 1996; received May 1, 1997; revision received Oct. 24, 1997; accepted for publication Oct. 24, 1997.

*Professor, Department of Aerospace and Ocean Engineering. Associate Fellow AIAA.
†Graduate Research Assistant, Department of Aerospace and Ocean Engineering. Student Member AIAA.
‡Associate Professor, Department of Aerospace and Ocean Engineering. Associate Fellow AIAA.

The active optics concept was first applied by Robertson et al.[1] to a 0.508-m-diam, three-segmented mirror. The mirror segments were aligned using three actuators per segment, which exerted control in piston and tilt only. Because the mirror segments were moved as rigid bodies, the elastic deformations could not be controlled using such control techniques. The concept of a thin deformable mirror was introduced by Robertson,[2] who investigated analytically and experimentally the feasibility of controlling the shape of a 0.762-m-diam, 0.0127-m-thick spherical mirror using actuators that worked on the rear surface of the mirror. Robertson used 58 equally spaced actuators to correct the surface error introduced during fabrication and mounting of the mirror on the reaction support system. A finite element model was utilized by Robertson to determine the actuator force configurations that would provide local displacements of the mirror at the actuator control points. The initial rms figure error, which was greater than 0.5 wavelength (6328 Å), was corrected to within 0.02 wavelength.

Creedon and Lindgren[3] employed the modal expansion technique to represent the surface distortion of a flexible structure in terms of its natural vibration modes and countered the distortion by exerting control over a finite number of most-significant modes. The actuators were located at the nodes of the next highest mode. They demonstrated this concept using a flat rectangular and circular plates for which mode shapes are available in closed forms. Howell and Creedon[4] extended the modal expansion method to a 0.7620-m-diam, 0.0127-m-thick spherical mirror used in the study by Robertson.[2] They used the first 58 modes for the modal expansion and 58 equally spaced actuators as in Ref. 1. The mode shapes were obtained using the finite element model as in Ref. 2. The actuator locations resulting in minimum surface error were selected from the common nodes of a predetermined number of uncontrolled modes. Ostroff[5] presented an improved method for selection of actuator locations based on minimization of the part of the potential energy that is associated with the uncontrolled modes. Ostroff[5] used the first 48 modes for the modal expansion of the surface distortion. The same finite element model that was used in Refs. 2–4 was employed, but all of the available nodal points were considered for positioning the actuators.

Scott[6] proposed a new method in which the correction of the surface distortion of the mirror is achieved by the application of moments at selected locations. An advantage of this method is that equal and opposite moments could be applied, eliminating the need for a rigid backup structure. Scott[6] used a finite element model of a 0.254-m flat disk to demonstrate the control of shapes in the form of the first 10 terms of the Zernike series, employing a maximum of 24 moment actuators.

Bushnell[7] studied the effectiveness of concentrated loads in controlling the surface distortions of 4-m-diam, 0.01-m-thick spherical caps and circular plates using a finite difference model. Two different distortions, one due to a nonuniform thermal field given in terms of a few terms of the Zernike series and the other consisting of Zernike polynomials themselves, were considered in his study. As many as 100 actuators were used to bring down the initial rms surface error by two orders of magnitude. Bushnell[7] found that mirrors with a very large diameter-to-thickness ratio and radius of curvature-to-thickness ratio are difficult to control.

Hansen et al.[8] presented an integrated active mirror system with 41 actuators in which a 4-m-diam, 0.02-m-thick spherical mirror was controlled in normal position, tangential slope, and radial slope. In their analytical study employing a finite element model, the actuator system was evaluated to control deformations due to a thermal gradient through the thickness, uniform thermal soak of the entire system, gravity loads, and optical aberrations such as defocus and astigmatism. Hansen et al.[8] also found that thick mirrors are easier to control than thin mirrors. They also came to interesting conclusions that deformations due to bending loads such as gravity or axial thermal gradient and deformations into shape of nondevelopable surface (defocus) are difficult to control, whereas deformations due to membrane loads such as a uniform rise in temperature and deformations into shapes of a developable surface (astigmatism) are easy to control.

Masaki et al.[9] performed shape control experiments using a 0.62-m-diam, 0.021-m-thick spherical mirror. They expressed the mirror deformations in the form of fundamental Zernike modes (astigmatism, coma, and spherical aberration) in terms of the first 24 normal modes of the mirror and controlled only 7 or 12 of the 24 observed modes using 9 force control actuators. The initial rms figure errors of the order of few hundred nanometers could be reduced to about 18 nm when 7 modes were controlled. When 12 modes were controlled, the residual rms error was about 72 nm.

In the majority of the aforementioned works, the surface deformations were controlled by applying forces at discrete locations on the rear surface of the mirror. A major drawback of using such discrete devices is the requirement of a rigid and, consequently, heavy support structure, which is undesirable for space applications. An alternative to this approach is to use piezoelectric actuators, which can be very lightweight and do not require a heavy backup structure. Kuo and Bruno[10] investigated the problem of determining the optimal locations of piezoelectric actuators to control surface distortions of a 1-m hexagonal flat panel using a modified simulated annealing technique. They used two types of distortions, one a linear combination of the first three normal modes and the other a linear combination of the first five normal modes, both having a maximum deformation of 5 μm in each mode. The optimization was performed several times using different starting configurations to determine the optimal configuration. They found that strips placed in the radial directions appeared in almost every run. Hence, a configuration with actuators placed along six radial lines resulting in 24 actuators was used to control both types of distortions. Using such a configuration, the rms error in the first case was reduced to 0.0305 μm and in the second case to 0.3529 μm. As can be seen from the results obtained by Kuo and Bruno,[10] the configuration of radially located piezoelectric actuators does not seem to be very effective in controlling complex surface distortions of the mirror segment.

In a subsequent study, Kuo[11] used a similar configuration with six radial groups of five actuators in each group to excite the first three natural modes of vibration of the panel and experimentally verified the numerical results obtained using the NASTRAN program. Using the same configuration, Kuo[12] performed experiments on a 0.5-m curved hexagonal mirror segment, 0.025 m thick with a radius of curvature of 7.6 m, demonstrating that, by applying different voltages to the six groups of actuators, the mirror could be deformed into shapes that are similar to the first eight Zernike polynomials.

Though the numerical and experimental work done by Kuo and Bruno[10] and Kuo[11,12] demonstrates the use of piezoelectric actuators to control the surface distortions of the mirror segment, the results presented do not give an indication of the effectiveness of the configuration of radially located actuators in controlling complex surface distortions of the mirror segment.

In the present work, control of thermal deformations of a 0.5-m hexagonal curved mirror segment, 0.012 m thick, with a radius of curvature of 10 m, using discrete and distributed actuators is presented. The mirror segment used is part of a multisegmented primary mirror of a next-generation space telescope.[13] A finite element model is used to represent the mirror–actuator system. To study the effectiveness of the discrete and distributed actuators, a comparative study is conducted using two different models of the mirror–actuator system. In model 1, the mirror is mounted on kinematic supports and controlled by piezoelectric strips that are bonded to the rear surface of the mirror. Two sets of strip configurations are studied: one with radially placed strips similar to that employed by Kuo and Bruno[10] and the other with evenly distributed strips. In model 2, the mirror is mounted on force actuators, which are used to support the mirror as well as to control the surface deformations of the mirror. The optimal values of the forces that are to be applied at the actuator control points and the voltages to be applied across the piezoelectric strips are determined by minimizing the rms surface figure error. A study is also conducted to compare the performance of evenly distributed strips with that of strips placed at near-optimal locations obtained using heuristic integer programming. Details of the analysis and the results are presented in the following sections.

Finite Element Model

The mirror is modeled using an assembly of thin flat triangular shell elements with six degrees of freedom (DOFs) per node. The flat shell element used is a combination of the discrete Kirchhoff theory (DKT) plate bending element with three DOFs per node (transverse displacement and two out-of-plane rotations) and a membrane element with three DOFs per node (two in-plane displacements and an in-plane rotation) similar to the Allman element but derived from the linear strain triangular element. The piezoelectric strip is modeled as a separate layer of isotropic material bonded to the lower surface of the mirror. For details regarding the finite element formulation, the reader is directed to Ref. 14, in which the flat shell element has been validated for linear analysis of composite plates and shells subject to mechanical, thermal, and electric loads. To demonstrate the correctness of the finite element formulation, an example of a square plate under an electric load (given in Ref. 14) is presented again, along with another example of a piezoelectric bimorph cantilever beam. Several examples of plates and shells under mechanical and thermal loads are presented in Ref. 14 and, hence, are not reproduced here.

Graphite/Epoxy Laminate Under an Electric Field

The plate is made of eight layers ($[0/90/0/90]_s$) of graphite/epoxy material and a ninth layer of piezoelectric polymer material, polyvinylidene fluoride (PVDF) twice as thick as the other eight layers. The plate is simply supported on two opposite edges and clamped on the other two edges. A constant voltage E_z (V/m) is applied across the PVDF layer. The geometry and the material properties used are those given by Jonnalagadda et al.[15] The convergence of the nondimensionalized center plate deflection is given in Table 1 along with the results of Jonnalagadda et al.[15] and are in good agreement.

Table 1 Convergence of nondimensionalized middeflection of a graphite/epoxy laminate excited by a uniform electric field

Grid size quarter plate	$100W(h/b)/(bd_{33}E_z)$
2×2	0.14042
4×4	0.13996
6×6	0.13962
8×8	0.13945
10×10	0.13936
12×12	0.13933
14×14	0.13927
16×16	0.13925
18×18	0.13924
Jonnalagadda et al.[15] 4×4 mesh (quarter plate), nine-node Lagrangian elements	0.1396

Table 2 Transverse deflection ($\times 10^7$) in meters of a piezoelectric bimorph cantilever beam under uniform electric field at different locations

Location:	2 cm	4 cm	6 cm	8 cm	10 cm
This study (1 × 20 mesh)	0.1376	0.5516	1.2416	2.2076	3.4496
Tzou and Tseng,[16] finite element method	0.124	0.508	1.16	2.10	3.30
Tzou and Tseng,[16] theory	0.138	0.552	1.24	2.21	3.45

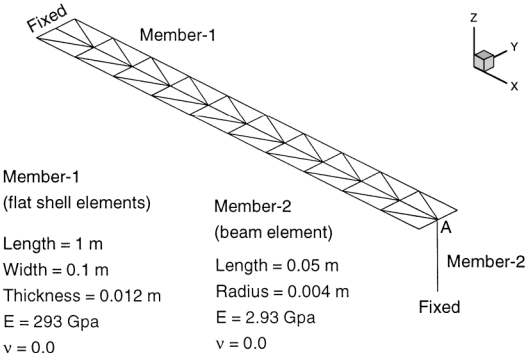

Fig. 1 Geometry and material properties of the L frame.

Piezoelectric Bimorph Cantilever Beam

The beam ($0.1 \times 0.005 \times 0.001$ m) is made of two layers of PVDF material with opposite polarity. A constant voltage of 1000 V/m is applied across the thickness. The material properties are the same as those used in the preceding example, except that Poisson's ratio used in this case is zero. A 1×20 mesh (40 elements and 42 nodes) was used to model the beam. The average of the transverse deflection at the nodes along the two edges of the beam at five locations along the beam are presented in Table 2, along with the analytical solution and finite element results (obtained using 10 solid isoparametric elements, 5 per layer) given by Tzou and Tseng.[16] The present results agree well with the analytical solution given by Tzou and Tseng. The finite elements results of Tzou and Tseng based on an isoparametric solid element formulation are stiffer than the analytical solution or the present results.

The force actuator is modeled using a two-node beam element.[17] The beam element has bending rigidity in two orthogonal planes normal to its longitudinal axis, extensional rigidity along its longitudinal axis, and torsional rigidity about its longitudinal axis, giving a total of six DOFs per node (three translations and three rotations). Shear deformations are also included in the beam formulation. One end of the actuator or the beam element is constrained in all DOFs to simulate the rigid backup structure, and the other end is connected to the mirror where the control force is applied. The reader is directed to Ref. 17 for details regarding the finite element formulation. The thermal deformations of the force actuators have not been considered in this study. Also, the thermoelastic coupling in the case of the mirror and the force actuators and the piezothermoelastic coupling in the case of the piezoelectric strips have not been considered.

The mirror–actuator model was verified using an example of an L frame fixed at the two ends and subject to concentrated forces P_x, P_y, and P_z at point A (Fig. 1) along the X, Y, and Z axes, respectively (Fig. 1), and a moment M_y at point A about the Y axis. The horizontal member (member 1) of the L frame was modeled using the flat shell elements with a Poisson ratio of zero, and the vertical member (member 2) was modeled using the beam element. The results were compared with those obtained using Castigliano's principle, those obtained by modeling the horizontal member using the B33 two-node Euler–Bernouli beam element and the vertical member using the B31 two-node Timoshenko beam element of the commercial finite element package ABAQUS, and those obtained by modeling horizontal member using the three-node flat shell element STRI3 of ABAQUS and vertical member using the B33 element. The STRI3 element of ABAQUS is a combination of the DKT plate bending element and the constant strain triangular element. The combination of STRI3 and B33 was used mainly to compare the in-plane deformations, as those obtained using the Castigliano's principle or the beam elements (B33 and B31) are not expected to agree with those obtained by modeling horizontal member using the shell elements. The results are presented in Table 3, where u_x, u_y, and u_z are the displacements along the X, Y, and Z axes, respectively. The present results are in good agreement with the rest of the results presented in Table 3, demonstrating the validity of the present mirror–actuator model.

Table 3 Deflection, in micrometers, at point A, of the L frame

Model	$P_x = 100$ N	$P_y = 100$ N	$P_z = 100$ N	$M_y = 100$ N
Present	$u_x = 0.291$	$u_x = 0$	$u_x = 0$	$u_x = 0.0257$
	$u_y = 0$	$u_y = 37.63$	$u_y = 0$	$u_y = 0$
	$u_z = 0$	$u_z = 0$	$u_z = 33.8$	$u_z = -50.6$
Theory	$u_x = 0.284$		$u_x = 0$	
	$u_y = 0$		$u_y = 0$	
	$u_z = 0$		$u_z = 33.8$	
B33+B31	$u_x = 0.284$		$u_x = 0$	
	$u_y = 0$		$u_y = 0$	
	$u_z = 0$		$u_z = 33.8$	
STRI3+B33	$u_x = 0.291$	$u_x = 0$	$u_x = 0$	$u_x = 0.0267$
	$u_y = 0$	$u_y = 37.59$	$u_y = 0$	$u_y = 0$
	$u_z = 0$	$u_z = 0$	$u_z = 33.8$	$u_z = -50.6$

Control Algorithm

The surface deformations of the mirror segment are corrected by applying control inputs to the force actuators and the piezoelectric strips, which act on the rear surface of the mirror. In the present study, control input for the force actuator is the concentrated force that is to be applied normal to the rear surface of the mirror at the grid points where the force actuator is attached to the mirror. In the case of the piezoelectric strips, the control input is the voltage to be applied across the thickness of the strip, which induces a distributed strain in the strip and, hence, in the mirror, assuming that the strips are perfectly bonded to the mirror. Because the number and locations of the force actuators and piezoelectric strips are predetermined, the shape control problem involves the determination of the optimum values of actuator forces or the voltages with which maximum possible correction can be obtained.

Consider a mirror approximated by m nodal points using the finite element model. Let ψ denote the deformed shape or the transverse displacements and u the correction to the transverse displacement applied in the opposite direction using n force actuators or piezoelectric strips. In this study, the deformed shape ψ is assumed to be known. The deformed shape or the mirror figure error can be estimated using the Shack–Hartmann wave front analyzer.[9] For details the reader is directed to Ref. 9 and the references therein. It suffices to mention here that the wave front analyzer estimates the deformed surface of the mirror by measuring the light emitted from the mirror. From the measurements made, the mirror surface is expressed in terms of Zernike polynomials using a suitable curve fit, and thus the mirror figure error at any location is available as a linear combination of the Zernike polynomials. Though the Zernike polynomials do not correlate to the mechanical characteristics of the mirror like the natural mode shapes, they have been widely used in the existing literature to represent the shape of the mirror. Masaki et al.[9] have shown that the lower Zernike modes are similar to the natural modes of a spherical mirror and, hence, the mirror deformations can be expanded in terms of the lower Zernike modes instead of the natural modes.

The correction u_i at any nodal point is given by

$$u_i = \sum_{j=1}^{n} \alpha_{ij} f_j \tag{1}$$

where the control input f_j is the force applied at the jth actuator location or the voltage applied across the jth piezoelectric strip and the influence coefficient α_{ij} is defined as the deformation caused at node i due to a unit force applied at the jth actuator alone or a unit voltage applied across the jth piezoelectric strip alone. It is

assumed that the material of the mirror, the force actuators, and the piezoelectric strips is linear elastic and isotropic. Because the deformations considered are of the order of a few micrometers, the geometric and material nonlinearitiesare less significant and, hence, the superposition used in Eq. (1) is justified.

A matrix of influence coefficients of size $m \times n$ is obtained from the finite element model by applying a unit load at each node where the actuator is attached to the mirror or by applying a unit voltage across each of the piezoelectric strips, one at a time. The correction u_i thus obtained, when applied on the deformed structure in the direction opposite to that of the desired shape ψ, tends to nullify the deformations. To obtain the best possible correction, the deviation from the desired shape should be made minimum at every point on the structure. Because the structure is modeled as a set of a finite number of nodal points, it is required that the deviation at these nodal points be minimum. A measure of the overall deviation or the rms figure error is given by

$$E = \sqrt{\frac{1}{m}\sum_{i=1}^{m}(\psi_i + u_i)^2} \tag{2}$$

Substituting Eq. (1) in Eq. (2), the rms error can be expressed in terms of the unknowns f_j as follows:

$$E = \sqrt{\frac{1}{m}\sum_{i=1}^{m}\left(\psi_i + \sum_{j=1}^{n}\alpha_{ij} f_j\right)^2} \tag{3}$$

setting $\partial E/\partial f_k = 0$ gives

$$\sum_{i=1}^{m}\left(\psi_i + \sum_{j=1}^{n}\alpha_{ij} f_j\right)\alpha_{ik} = 0, \qquad k = 1, 2, \ldots, n \tag{4}$$

Equation (4) is of the form $[A]\{f\} = \{b\}$, where

$$A_{kj} = \sum_{i=1}^{m}\alpha_{ij}\alpha_{ik}, \qquad b_k = -\sum_{i=1}^{m}\psi_i\alpha_{ik}$$

The solution of this set of equations, obtained using the standard LDL^T direct factorization, gives the values of control inputs for which best possible correction can be obtained. Because the material is assumed to be linear elastic, the control inputs thus obtained are those that cause the undeformed mirror to deform to the shape given by ψ. The control inputs thus obtained will have to be applied in the opposite direction, on the deformed mirror, to obtain the necessary correction.

The control algorithm was validated by using the deformed shape due to arbitrary loads applied at a few nodal points and that due to arbitrary voltages applied across a few piezoelectric strips. The magnitude of the optimum forces and the voltages obtained using the control algorithm were exactly the same as those used to generate the deformed shape but of opposite sign.

Results and Discussion

The aforementioned algorithm is applied to control the thermal deformations of a spherical mirror segment with a hexagonal base. The geometry and material properties of the mirror, piezoelectric strip,[18] and force actuator are given in Table 4. The temperature distribution at the lower surface of the mirror is assumed to be in the form of linear combination of the first few terms of the Zernike series[19] expressed in terms of Cartesian coordinates x and y with the origin at the center of the mirror. The Cartesian coordinates used to express the temperature distributions are normalized such that they are in the range $[-1, 1]$. The temperature distributions that are considered in this study are given in Table 5, where the constant C is used to scale the temperature distributions such that the upper, light-reflecting surface is at a lower temperature than the lower surface, with a constant temperature difference ΔT_z°C, and the maximum temperature difference between any two grid points across the lower surface of the mirror is ΔT_{xy}°C.

Table 4 Properties and geometry of the mirror, piezoelectric strip, and force actuator

Property/geometry	Mirror (beryllium)	Piezoelectric strip	Force actuator
Young's modulus, GPa	293	63	2.93
Poisson ratio	0.1	0.3	0.1
Coefficient of thermal expansion, /°C	11.5E-6	0.9E-6	
Thickness, m	0.012	0.25E-3	
Radius of curvature, m	10		
Side of the hexagonal base, m	0.5		
d_{31}, d_{32}, m/V		254E-12	
Diameter, m			0.008
Length, m			0.05

Table 5 Temperature distribution at the lower surface of the mirror

T1	$C[2(x^2 + y^2) - 1]$
T2	$C[(x + y)(3x^2 + 3y^2 - 2)]$
T3	$C\left(\sum_{i=1}^{i=9} K_i Z_i\right)$ K_i from Table 2 (back surface) of Ref. 19
T4	$C[x + y + 2xy]$

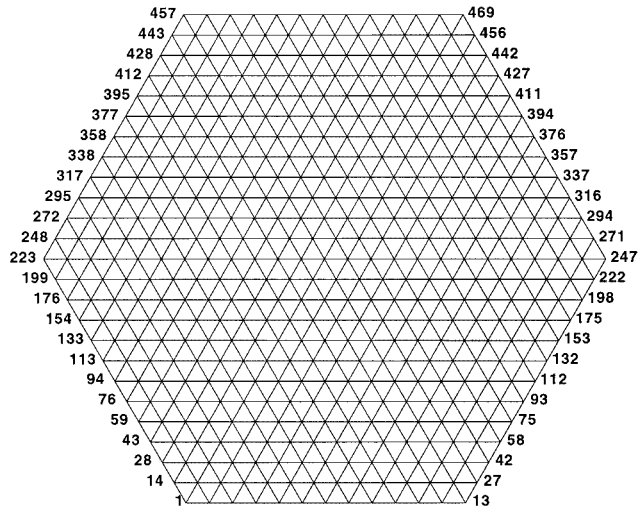

Fig. 2 Finite element mesh for model 1 (node numbers).

The finite element mesh for model 1 (Fig. 2) consists of 864 flat shell elements and 469 grid points. The mirror in model 1 is supported at the six vertices 1, 13, 223, 247, 457, and 469. The translational DOFs are constrained at the supports. It is preferable to support the mirror on all six vertices than on three vertices 120 deg apart. This is because the edge deformations in the former case resemble those of a simply supported beam and are easier to correct than the cantilever-type deformations along the edges in the latter case. The thermal deformations are controlled using piezoelectric strips bonded to the lower surface of the mirror. Two sets of configuration of the strips are considered: one with 30 radially placed strips (Fig. 3) similar to the configuration used by Kuo and Bruno[10] and the other with 121 evenly distributed strips (Fig. 3). It was observed that better control could be achieved by adding strips near the periphery to a set of 79 evenly distributed strips (Fig. 3), resulting in a set of 121 evenly distributed strips as shown in Fig. 3. Because the piezoelectric strips are very light and flexible, a large number of such strips can be used without drastically increasing the overall weight or stiffness of the mirror, unlike the conventional force actuators. The configuration of 121 strips, shown in Fig. 3, consists of 37 hexagonal strips and 84 semihexagonal strips. Each hexagonal strip has a side of 0.04166 m. The optimal locations are determined from a starting configuration of 193 strips (Fig. 3) consisting of 91 hexagonal strips and 102 semihexagonal strips. The

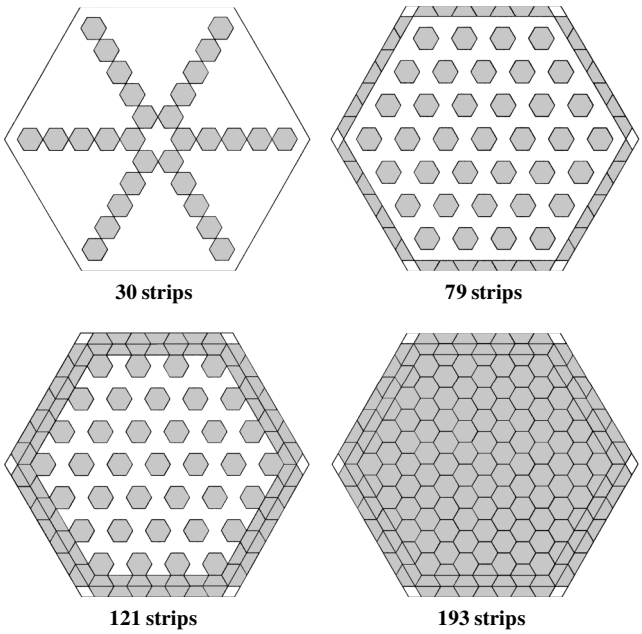

Fig. 3 Piezoelectric strip configurations.

heuristic algorithm used to determine the (near) optimal locations is described later in this section.

In the case of radially placed and evenly distributed strips, the influence coefficients are determined by applying a unit voltage across each strip, one at a time, in the presence of all other strips. To determine the optimal locations of the strips, an approach similar to that followed by Kuo and Bruno[10] is used. The influence coefficients are first determined by neglecting the stiffness of the strips in computing the global stiffness matrix. If the stiffness of the strips is included in the global stiffness matrix for determining the influence coefficients, each set of influence coefficients would correspond to a different global stiffness matrix and, hence, the linear combination of the sets of influence coefficients thus obtained will not correspond to any one stiffness matrix. In other words, the influence coefficients are determined by applying a unit voltage across each of the strips, one at a time, in the absence of the rest of the strips.

The optimal locations of the strips are obtained using the Dlorenzo algorithm.[20] This algorithm was chosen because it does not require any initial guess locations as in other optimization techniques such as simulated annealing.[10] More exhaustive integer programming methods are available in the literature,[20] but they are computationally much more expensive than the Dlorenzo algorithm and they also have a certain degree of uncertainty due to the requirement of initial guess locations.

The Dlorenzo algorithm starts with an initial configuration of 193 strips, as shown in Fig. 3. The steps followed in the algorithm are as follows. 1) Remove each of the strips from the initial configuration of n strips ($n = 193$) one at a time, and determine the rms error due to n configurations of $n - 1$ strips. 2) Rank the strips in ascending order of the rms error. 3) Remove the strip that results in the smallest rms error, to obtain a new configuration of $n - 1$ strips. 4) Repeat steps 1–3 until the desired number (30 or 121) of strips is reached. The configuration thus obtained is called the optimal configuration in the subsequent sections, though it is certainly not the best possible configuration.

The thermal deformations of model 1 are computed by neglecting the stiffness of the strips. The rms and absolute values of the transverse deformation of model 1 without the strips and with 30 and 121 strips are given in Table 6 for $\Delta T_z = 0.2^\circ$C and $\Delta T_{xy} = 0.5^\circ$C. As can be seen from Table 6, there is not much difference in the rms and absolute maximum deformations of the mirror without the strips and with 30 and 121 strips. This can be attributed mainly to the fact that the thickness and the stiffness of the strips are much lower than those of the mirror. Hence, neglecting the stiffness of the strips in determining the optimal locations is not expected to give erroneous results. Moreover, as the deformed shape of the mirror without the strips did not vary significantly from that in the presence of the strips, the optimal locations could be used to control the deformed shape in the presence of the strips. After determining the optimal locations, the influence coefficients are computed now by including the stiffness of the strips as done in the case of radial and evenly distributed strips.

Table 6 Uncorrected rms and maximum absolute values of the transverse deformations of model 1, in micrometers, due to different temperature distributions

	Without strips		With 30 strips		With 121 strips	
$T(x, y)$	rms	Absolute	rms	Absolute	rms	Absolute
T1	4.85	9.65	5.01	9.89	5.00	9.88
T2	3.00	5.27	3.14	5.49	3.11	5.47
T3	1.89	4.91	1.89	4.87	1.87	4.81
T4	3.28	5.68	3.39	5.89	3.37	5.86

Table 7 Corrected rms and maximum absolute residual values of the transverse deformations of model 1, in micrometers, due to different temperature distributions

	30 radially placed strips		30 optimally placed strips	
$T(x, y)$	rms (%)	Absolute (%)	rms (%)	Absolute (%)
T1	0.556 (11.5)	1.868 (19.3)	0.201 (4.1)	0.686 (7.1)
T2	0.749 (24.9)	2.698 (51.2)	0.220 (7.3)	0.884 (16.8)
T3	0.795 (42.0)	3.822 (77.8)	0.199 (10.5)	0.883 (17.9)
T4	0.924 (28.1)	3.578 (62.9)	0.217 (6.6)	0.840 (14.9)

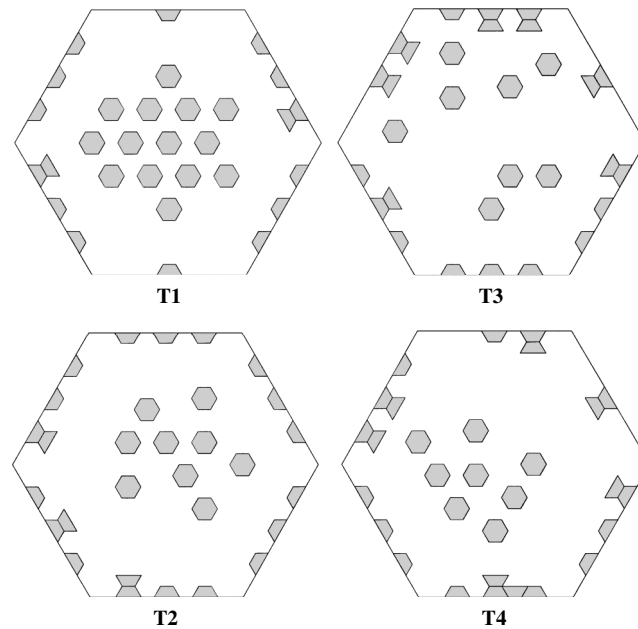

Fig. 4 Optimal locations of 30 strips.

The corrected rms figure error and the maximum residual deformations for model 1 using 30 radially placed strips and 30 optimally placed strips for $\Delta T_z = 0.2^\circ$C and $\Delta T_{xy} = 0.5^\circ$C are given in Table 7. The optimal voltages to be applied to 30 strips varied from -558 to 389 V in the case of radially placed strips, and in the case of optimally placed strips the voltages varied from -1312 to 853 V. The negative sign indicates that the voltage is applied in the direction opposite to the direction of polarization of the piezoelectric material. The corrected rms figure error and the maximum residual deformations for model 1 using 121 evenly placed strips and 121 optimally placed strips for $\Delta T_z = 0.2^\circ$C and $\Delta T_{xy} = 0.5^\circ$C are given in Table 8. The optimal voltages to be applied to 121 strips varied from -983 to 547 V in the case of evenly placed strips, and in the case of optimally placed strips the voltages varied from -1159 to 1242 V. The optimal locations of 30 and 121 strips are shown in Figs. 4 and 5, respectively.

Table 8 Corrected rms and maximum absolute residual values of the transverse deformations of model 1, in micrometers, due to different temperature distributions

	121 evenly distributed strips		121 optimally placed strips	
$T(x, y)$	rms (%)	Absolute (%)	rms (%)	Absolute (%)
T1	0.081 (1.7)	0.256 (2.7)	0.058 (1.2)	0.197 (2.0)
T2	0.093 (3.1)	0.255 (4.9)	0.075 (2.5)	0.248 (4.7)
T3	0.088 (4.6)	0.307 (6.3)	0.070 (3.7)	0.246 (5.0)
T4	0.098 (3.0)	0.309 (5.4)	0.079 (2.4)	0.223 (3.9)

Table 9 Uncorrected and corrected rms values of the transverse deformations of model 1, in micrometers, due to different temperature distributions

$T(x, y)$	Uncorrected rms	Corrected rms (%)
T1	1.971	0.0239 (1.2)
T2	0.536	0.0147 (2.7)
T3	2.125	0.0278 (1.3)
T4	1.195	0.0285 (2.4)

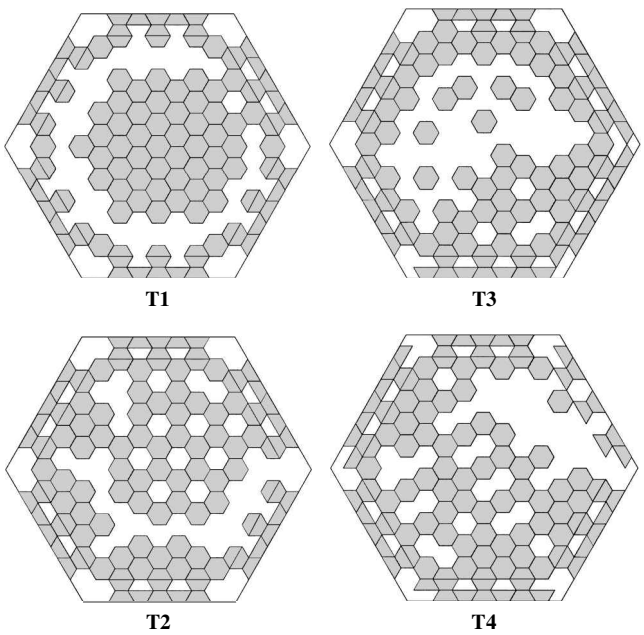

Fig. 5 Optimal locations of 121 strips.

The surface distortions could not be reduced much using 30 radially placed strips. The poor performance of 30 radially placed strips can be attributed to the fact that the influence of the strips is restricted to a certain area, unlike the case of evenly distributed strips. Even using 30 (near) optimally placed strips, the percentage reduction in the rms figure error or the maximum residual deformation seems insufficient in the case of complex deformations T2 and T3 (Table 7). The performance of 121 evenly distributed strips (Table 8) is quite close to that of 121 (near) optimally placed strips. The amount of correction obtained in the case of asymmetric thermal fields T2, T3, and T4 indicates that the performance of 121 evenly distributed strips is not biased toward symmetric deformations or symmetric support conditions. The corrected rms values given in Table 8 for 121 evenly distributed strips range from 81 to 97 nm. The rms figure error of the surface distortions of the mirror segment of the next-generation space telescope[13] should be within $\frac{1}{20}$th of the operating wavelength (0.5 μm) to achieve satisfactory optical performance. By restricting ΔT_z to 0.025°C and ΔT_{xy} to 0.4°C, the initial rms figure errors ranging from about 0.5 to 2.1 μm could be reduced to within 29 nm, using 121 evenly distributed strips (Table 9). The optimum voltages applied to 121 evenly distributed strips in this case range from −290 to 238 V (−1.16 to 0.95 MV/m).

Table 10 Uncorrected and corrected rms and maximum absolute values of the transverse deformations of model 2, in micrometers, due to different temperature distributions, using 61 force actuators

	Uncorrected		Corrected	
$T(x, y)$	rms	Absolute	rms (%)	Absolute (%)
T1	0.5228	1.1997	0.0444 (8.5)	0.0954 (7.9)
T2	0.9456	2.4391	0.0414 (4.4)	0.0946 (3.8)
T3	1.1800	2.8037	0.0407 (3.4)	0.0942 (3.4)
T4	0.9212	2.1236	0.0413 (4.5)	0.0915 (4.3)

Table 11 Uncorrected and corrected rms values of the transverse deformations of model 2, in micrometers, due to different temperature distributions, using 61 force actuators

$T(x, y)$	Uncorrected rms	Corrected rms (%)
T1	0.5119	0.0078 (1.5)
T2	0.2062	0.0054 (2.6)
T3	0.3802	0.0050 (1.3)
T4	0.1153	0.0052 (4.5)

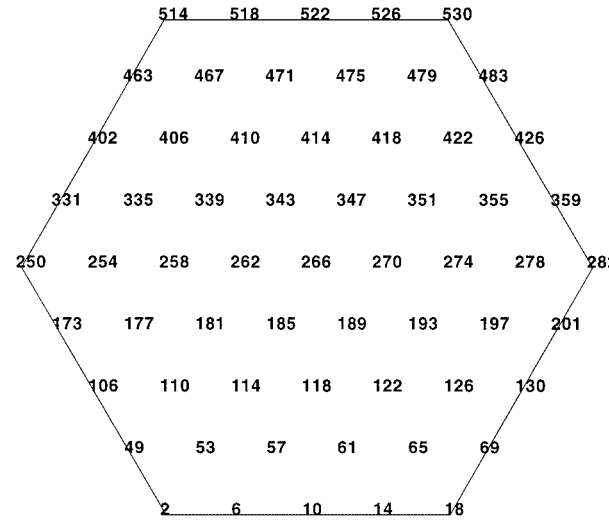

Fig. 6 Locations of 61 force actuators.

The finite element mesh for model 2 consists of 864 flat shell elements and 61 beam elements. The mirror is mounted on 61 force actuators (Fig. 6), which are used to support the mirror as well as to control the surface deformations of the mirror. The actuators are placed with an equal interactuator distance of 0.125 m. One end of the actuators or beam elements is constrained in all six DOFs, and the other end is attached to the mirror. Young's modulus of the actuators is assumed to be $\frac{1}{100}$ of that of the mirror. The uncorrected and corrected rms and maximum absolute values of the transverse deformations of model 2, in micrometers, due to different temperature distributions for $\Delta T_z = 0.2$°C and $\Delta T_{xy} = 0.5$°C are given in Table 10. The optimum actuator forces applied to actuators in this case varied from −34 to 20.4 N. The uncorrected and corrected rms values for $\Delta T_z = 0.025$°C and $\Delta T_{xy} = 0.4$°C are given in Table 11. The optimum actuator forces applied to actuators in this case varied from −6.4 to 9 N.

Because the actuators are used for both support and control, changing the location of the actuators will result in different support configurations and, hence, different thermal deformations. In other words, the problem does not remain the same when changing the locations of the actuators. Therefore, no attempt is made to determine the optimal locations.

The thermal deformations in the case of model 2 are smaller than those of model 1 due to the obvious fact that the mirror is more constrained in model 2 than in model 1. Except T1, the corrected rms figure errors obtained using 61 force actuators are quite close to that obtained using 121 piezoelectric actuators for $\Delta T_z = 0.2$°C

and $\Delta T_{xy} = 0.5°C$. The thermal deformation due to the temperature distribution T1 resembles that of defocus, which can be corrected using a focal plane correction system[9] without using force actuators or piezoelectric strips. When ΔT_z is reduced to 0.025°C and ΔT_{xy} to 0.4°C, the percentage reduction in the rms error obtained using 61 force actuators is quite close to that obtained using 121 piezoelectric strips for all four of the temperature distributions. The corrected rms in the case of the force actuators (Table 11) is much lower as the uncorrected rms is also much lower than those in the case of the piezoelectric strips.

Conclusion

Active control of thermal deformations of a thin hexagonal spherical mirror segment using discrete and distributed actuators was presented. A finite element model was used to represent the mirror–actuator system. To determine the effectiveness of the actuators in controlling the surface distortions of the mirror, a comparative study was performed using two different models of the mirror-actuator system. In model 1, the mirror was mounted on kinematic supports and the thermal deformations were controlled using piezoelectric strips that were bonded to the rear surface of the mirror. In model 2, the mirror was mounted on force actuators, which were used to support the mirror as well as to control the surface distortions of the mirror. A study was also performed to compare the performance of evenly distributed strips with that of strips placed at near optimal locations obtained using heuristic integer programming.

Both the force actuators and the piezoelectric strips were equally effective in controlling the surface deformations of the mirror. The performance of 121 evenly distributed strips was quite comparable to that of 121 optimally placed strips. Mounting the mirror on a large number of force actuators (model 2) appeared to be more advantageous than supporting the mirror on six kinematic supports (model 1) at the vertices because the mirror deformations in the former were much lower than those in the latter, but a disadvantage of using the force actuators is the increase in the overall weight of the structure, which is undesirable for space applications. Because the piezoelectric strips are lightweight, a large number of such strips can be used to control the surface distortions of the mirror without imposing a weight penalty. Piezoelectric strips can also be used to correct both developable and nondevelopable surfaces because they, unlike the force actuators, can be used to impart both membrane and bending strains on the mirror.

In the actual mirror, the piezoelectric strips cannot be relocated as they will be bonded to the rear surface of the mirror. Moreover, the optimal locations determined for one type of disturbance may not be optimal for other disturbances. Correcting the mirror deformations using a set of strips with predetermined locations thus seems to be more practical than trying to find the optimal locations. Controlling the mirror deformations using a large number of evenly placed piezoelectric strips seems to be a viable solution as such a configuration can impart control to almost every part of the mirror and, hence, can be used to control arbitrary deformations.

Because the piezoelectric strips act over a finite area of the mirror and the force actuators only act discretely, the mirror surface corrected using the former is expected to be smoother than that corrected using the latter. The quality of the mirror surface should be assessed to determine whether the mirror surface is smooth enough to obtain the required operational efficiency. The rms figure error may not be a true measure of surface smoothness. Hence, alternative measures to assess the surface smoothness of the mirror have to be determined.

It may not be possible to generate in space the kind of voltages, as determined in this study, that are to be applied to the piezoelectric strips. Hence, there is a need for piezoelectric materials with much higher strain constants. A parametric study can also be conducted to determine the optimum values of the stiffness and the dimensions of the mirror and the piezoelectric strips that will result in the smallest thermal deformations and voltages to be applied across the strips. The feasibility of using a large number of piezoelectric strips on a mirror segment should also be examined because the use of a large number of strips could result in a very complex electronic circuitry. In summary, the piezoelectric strips appear to be promising candidates for static shape control of flexible structures in space, opening several avenues for further research to determine the feasibility of using a large number of such strips for practical problems.

Acknowledgment

The authors wish to acknowledge the support by NASA under Grant NAGW-4241.

References

[1]Robertson, H. J., Crane, R., and Hemstreet, H. S., "Active Optics System for Spaceborne Telescopes," NASA CR-66297, Oct. 1966.

[2]Robertson, H. J., "Development of an Active Optics Concept Using a Thin Deformable Mirror," NASA CR-1593, 1970.

[3]Creedon, J. F., and Lindgren, A. G., "Control of the Optical Surface of a Thin Deformable Primary Mirror with Application to an Orbiting Astronomical Observatory," *Automatica*, Vol. 6, 1970, pp. 643–660.

[4]Howell, W. E., and Creedon, J. F., "A Technique for Designing Active Control Systems," NASA TND-7090, Jan. 1973.

[5]Ostroff, J. A., "Evaluation of Control Laws and Actuator Locations for Control Systems Applicable to Deformable Astronomical Telescope Mirrors," NASA TND-7276, Oct. 1973.

[6]Scott, R. M., "New Technique for Controlling Optical Mirror Shapes," *Optical Engineering*, Vol. 14, 1975, pp. 112–115.

[7]Bushnell, D., "Control of Surface Configurations of Nonuniformly Heated Shells," *AIAA Journal*, Vol. 17, No. 1, 1979, pp. 78–84.

[8]Hansen, J. G. R., Richard, R. M., and Shannon, R. R., "Deformable Primary Mirror for a Space Telescope," *Applied Optics*, Vol. 21, 1982, pp. 2620–2630.

[9]Masaki, T., Noboru, I., Keizo, M., Atsushi, S., Masanori, I., Yasumasa, Y., Takeshi, N., and Wataru, T., "Shape Control Experiments with a Functional Model for Large Optical Reflectors," *First Joint U.S./Japan Conference on Adaptive Structures* (Maui, HI), Technomic, Lancaster, PA, 1990, pp. 615–630.

[10]Kuo, C. P., and Bruno, R., "Optimal Actuator Placement on an Active Reflector Using a Modified Simulated Annealing Technique," *First Joint U.S./Japan Conference on Adaptive Structures* (Maui, HI), Technomic, Lancaster, PA, 1990, pp. 1056–1067.

[11]Kuo, C. P., "Adaptive Optics—One Meter Deformable Composite Mirror," *AIAA 32nd Structures, Structural Dynamics, and Materials Conference* (Baltimore, MD), 1991, AIAA, Washington, DC, pp. 1611–1617; also AIAA Paper 91-0907, April 1991.

[12]Kuo, C. P., "Optical Tests of an Intelligently Deformable Mirror for Space Telescope Technology," *Proceedings of the SPIE — The International Society for Optical Engineering*, Vol. 2040, 1993, pp. 631–646.

[13]Jakubowski, A. K., Mohan, P., Kapania, R. K., Crissafulli, P., and Hammerand, D., "8-m UV/Visible/IR Space Telescope," *Proceedings of SPIE—The International Society for Optical Engineering*, Vol. 2478, 1995, pp. 20–34.

[14]Kapania, R. K., and Mohan, P., "Static, Free Vibration and Thermal Analysis of Composite Plates and Shells Using a Flat Triangular Shell Element," *Computational Mechanics*, Vol. 17, No. 5, 1996, pp. 343–357.

[15]Jonnalagadda, K. D., Blandford, G. E., and Tauchert, T. R., "Piezothermoelastic Composite Plate Analysis Using First-Order Shear Deformation Theory," *Computers and Structures*, Vol. 51, 1994, pp. 79–89.

[16]Tzou, H. S., and Tseng, C. I., "Distributed Dynamic Identification and Controls of Flexible Shells," *AIAA 31st Structures, Structural Dynamics, and Materials Conference* (Long Beach, CA), AIAA, Washington, DC, 1990, pp. 2265–2273; also AIAA Paper 90-1089, April 1990.

[17]Hughes, O. F., *Ship Structures Design—A Rationally Based Computer Aided Optimization Approach*, Society of Naval Architects and Marine Engineers, 1988.

[18]Ha, S. K., Keilers, C., and Chang, F. K., "Finite Element Analysis of Composite Structures Containing Distributed Piezoceramic Sensors and Actuators," *AIAA Journal*, Vol. 30, 1992, pp. 772–780.

[19]Pearson, E., and Stepp, L., "Response of Large Optical Mirrors to Thermal Distributions," *Proceedings of SPIE—The International Society for Optical Engineering*, Vol. 748, 1987, pp. 215–228.

[20]Haftka, R. T., and Adelman, H. M., "Selection of Actuator Locations for Static Shape Control of Large Space Structures by Heuristic Integer Programming," *Computers and Structures*, Vol. 20, 1985, pp. 572–582.

H. L. McManus
Associate Editor